Bias and Trend Correction of Precipitation Datasets to Force Ocean Models

RAPHAEL DUSSIN[a,b]

[a] *University Corporation for Atmospheric Research, Boulder, Colorado*
[b] *NOAA/OAR/Geophysical Fluid Dynamics Laboratory, Princeton, New Jersey*

(Manuscript received 18 January 2022, in final form 13 July 2022)

ABSTRACT: A novel method to adjust the precipitation produced by atmospheric reanalyses using observational constraints to force ocean models is described. The method allows the preservation of the qualities of the high-resolution and high-frequency output from the reanalyses while eliminating their bias and spurious trends. The method is shown to be robust to degradation in both space and time of the observation dataset. This method is applied to the ERA-Interim precipitation dataset using the Global Precipitation Climatology Project (GPCP) v2.3 as the observational reference in order to create a debiased dataset that can be used to force ocean models. The produced debiased dataset is then compared to ERA-Interim and GPCP in a suite of forced ice–ocean numerical experiments using the GFDL OM4 model. Ocean states obtained with the new precipitation dataset are consistent with results from GPCP-forced experiments with respect to global metrics but produces the extra sea surface salinity variability at the time scales unresolved by the observation-based dataset. Discrepancies between modeled and observed freshwater fluxes are discussed as well as the strategies to mitigate them and their impacts.

KEYWORDS: Atmosphere-ocean interaction; Precipitation; Ocean models; Reanalysis data

1. Introduction

Present-day atmospheric reanalyses produced by major research centers, e.g., European Centre for Medium-Range Weather Forecast (https://ecmwf.int), NOAA National Centers for Environmental Predictions (https://ncep.noaa.gov), NASA Global Modeling and Assimilation Office (https://gmao.gsfc.nasa.gov/), and Japan Meteorology Agency (http://jma.go.jp), provide ocean modelers with very valuable datasets to force ocean general circulation models. The ever-increasing spatial and temporal resolution of these reanalyses allow them to represent a wider spectrum of dynamical features and make them essential assets for oceanographers to understand the impact of multiscale atmospheric variability on the ocean circulation and/or provide the most realistic surface boundary conditions to their ocean models.

Over the past decades, atmospheric models and data assimilation techniques have made great progress and the number of observations available for these reanalyses greatly increased. In spite of this, precipitation is still a difficult quantity to accurately represent because of all the physical processes involved: Stephens et al. (2010) showed that rainfall in major weather and climate models is still showing severe discrepancies with observations and more recently Tapiador et al. (2019) discussed the usefulness of precipitation as a metric for model evaluation and describes it as a "tough test for model performance." Atmospheric reanalyses share the same code base with the aforementioned models and hence some of their flaws, such as the "drizzle effect" (Dai 2006), despite the use of sophisticated algorithms to assimilate observations. Precipitation in first-generation reanalyses, such as NCEP-R2 (Kanamitsu et al. 2002) or ERA-40 (Uppala 2001), were so problematic that they could not be used to force ocean models. Figure 1 shows the global mean precipitation in some of the most used reanalyses compared to the GPCP v2.3 (Adler et al. 2003) observational product. Not only do NCEP-R2 and ERA-40 overestimate average precipitation by as much as 0.6 mm day^{-1}, they also exhibit large spurious trends and excessive interannual variability (respectively, 0.12 and 0.26 mm day^{-1} in standard deviation) compared to the GPCP estimate of 0.02 mm day^{-1}. In the dataset provided for the Coordinated Ocean-Ice Reference Experiment (Griffies et al. 2009), Large and Yeager (2009) use a spatial blend of early GPCP and CMAP (Xie and Arkin 1997) observation-based datasets labeled GXGXS, which is then adjusted to balance the evaporation–precipitation–runoff (E–P–R) budget with a gain and bias: $P_{\mathrm{CORE}} = 1.1417 \times P_{\mathrm{GXGXS}} + 0.7$ (mg m^{-2} s^{-1}) [see Large and Yeager (2004) for details]. This procedure, oftentimes ad hoc, is necessary to minimize drifts in salinity and sea surface height in the ocean model and the amplitude of the correction can be computed using observed or modeled evaporation. The precipitation in the CORE dataset is about 0.1 mm day^{-1} stronger on average than GPCP due to the E–P adjustments but its interannual variability over the period 1979–2007 is close to GPCP at 0.03 mm day^{-1}. CORE precipitation is not available after 2007. Similarly, ERA-40-based DRAKKAR Forcing Sets (hereafter DFS; see Brodeau et al. 2010) either use CORE precipitation unaltered in DFS v3 or with minor adjustments (+10% in the equatorial band, +5% elsewhere) in DFS v4 rather than using precipitation produced by ERA-40.

The following generation of atmospheric reanalyses provide more suitable precipitation but strong tuning is still necessary to remedy the spurious trends and biases. Although ERA-Interim performs much better than its predecessor, it is still overestimating the average precipitation rate by an average 0.24 mm day^{-1} and the interannual variability by a factor

Corresponding author: Raphael Dussin, raphael.dussin@noaa.gov

DOI: 10.1175/JTECH-D-22-0007.1

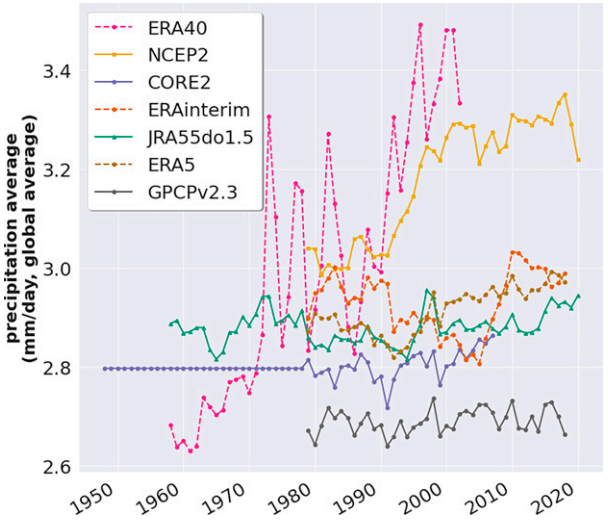

FIG. 1. Precipitation rates (mm day^{-1}, global average) in various atmospheric reanalyses and GPCP estimates. First-generation reanalyses (ERA-40, NCEP-R2) suffered large biases and trends; CORE2 and JRA55-do1.5 have corrections toward observations. All reanalyses produce precipitation stronger than GPCP v2.3 observational estimates.

of 2. It also exhibits spurious trends shown in Fig. 24 of Dee et al. (2011) and traced back to an issue with the 1D+4D-Var rain assimilation scheme. In the DFS v5 forcing (Dussin and Barnier 2013), ERA-Interim precipitation need to be detrended over 3 successive periods (1979–91, 1992–2004, and 2005–12) and then rescaled to the 30-yr average before spatial corrections are applied. The JRA55-do forcing (Tsujino et al. 2018), prepared for the second phase of the Ocean Model Intercomparison Project (Tsujino et al. 2020), heavily rectifies the original JRA-55 reanalysis. Adjustments to the precipitation are applied using spatially varying multiplying factors for each month, over 4 different periods (phases) and using either CORE or GPCP v2.3 as reference. With this procedure, the resulting precipitation are still about 0.08 mm day^{-1} stronger than CORE but with no noticeable trend and comparable interannual variability. Although the aforementioned methods produce precipitation datasets that work for their intended applications, the corrections developed there are both tedious to build and difficult to justify scientifically. The latest reanalysis from ECMWF, ERA5 has a 0.25° horizontal resolution and is presented as having greatly improved over ERA-Interim. Although the interannual variability in global precipitation is reduced to 0.04 mm day^{-1}, it exhibits a decline in global precipitation of about 0.05 mm day^{-1} during the first 13 years, followed by a steady increase resulting in an additional 0.15 mm day^{-1} after the next 3 decades. This behavior suggests that the need for adjustment of precipitation will remain for the foreseeable future.

One could be tempted to only use observation-based precipitation datasets to force an ocean model. Unfortunately the few global datasets, such as GPCP and CMAP, only have a horizontal resolution of 2.5° and monthly estimates. This is far coarser in time and space than what reanalyses can provide and hence do not provide the same level of detail than what is sought by ocean modelers. Other observational products, such as TRMM (Huffman et al. 2007), offer a higher resolution and temporal frequency but are limited geographically which restricts its use to regional models comprised between 35°N and 35°S. Ideally one would keep the level of detail that a modern reanalysis can offer while being consistent with observed values. Killworth (1996) showed that the linear interpolation of monthly forcing fields, as performed in ocean models, lead to errors in the applied fluxes. Precipitation is a critical contributor to ocean salinity variability, in particular in regions of intense activity such as the tropics (Delcroix et al. 1996). Because the seawater equation of state is nonlinear with respect to salinity, the frequency at which the freshwater fluxes are applied to an ocean model have the potential to change the circulation. Evaporation and momentum fluxes are typically computed using wind and air humidity surface boundary conditions given with periods ranging between an hour to 6 h. Using the slow-changing monthly precipitation in conjunction with the rapidly varying evaporation could lead to inconsistencies and imbalances, especially during atmospheric convection events. Modifying the precipitation from a reanalysis to force an ocean model is a balancing act aiming at rectifying averages toward observed values without degrading the spatial and temporal resolution of the original dataset. Closing the freshwater budget is also an important consideration depending on the ocean model used and the purposes it is used for.

This article demonstrates a new method to produce adjusted precipitation datasets, in a way that preserves the spatiotemporal resolution of the original reanalysis product while using observational constraints to eliminate both biases and spurious trends. The method is applied on the ERA-Interim reanalysis precipitation data using GPCP v2.3 as the observational constraint. The method is not limited to these two particular datasets and can be applied to any combination of modeled and observed precipitation. ERA-Interim is a good candidate to demonstrate the method because of the aforementioned bias and spurious trends and GPCP v2.3 is the only global dataset that covers the 1979–2018 period. The method is further tested for robustness in the case of degraded observational constraints and the produced precipitation dataset is then used to force the GFDL OM4 global ocean model at 0.5° horizontal resolution to assess the impact of the method on freshwater fluxes and modeled sea surface salinity.

2. Methodology

The typical strategy for debiasing precipitation datasets produced by atmospheric reanalyses is to make adjustments to the original reanalysis data, using available observational datasets. Such adjustments are often based on the annual or monthly mean (or zonal mean) precipitation rates in the reanalysis and observations over the whole length of the datasets or subintervals like in Tsujino et al. (2018). The obtained spatially varying multiplicative ratio is then applied to all the records of the considered interval. This approach assumes some

level of spatiotemporal stationarity in the bias. Attempts to detrend original precipitation require a great deal of arbitrary choices in terms of methods, time periods considered and observational datasets used. The method envisioned here is to start from an observational dataset for which we have reasonable confidence in the mean precipitation rate and time evolution, which solves the spurious trend problem. The observational dataset is then augmented with spatiotemporal variability from the reanalysis. This involves remapping the observations to the grid resolution of the reanalysis and adding the high-frequency variability in a way that respects the monthly totals at each grid point of the original observations. The details of the algorithm are as follows:

1) All computations are done at the frequency of the observational dataset (e.g., monthly).
2) The observational dataset is spatially remapped onto the horizontal grid of the reanalysis, which has a higher resolution, with a first-order conservative scheme using the ESMF library (Hill et al. 2004).
3) For each given period (e.g., month), the cumulative sum of the precipitation rate in the reanalysis data is computed then normalized by the sum over the period (i.e., total modeled precipitation):

$$\mathrm{HF}_{\mathrm{model}}(t) = \frac{1}{\sum_{k=1}^{T} \mathrm{PR}_{\mathrm{model}}(k)\,\Delta t} \times \sum_{k=1}^{t} \mathrm{PR}_{\mathrm{model}}(k)\,\Delta t, \qquad (1)$$

with $\mathrm{PR}_{\mathrm{model}}$ the precipitation rate of the model as a function of time t, T is the length of the period (e.g., 1 month), and k the time increment (e.g., 1 day). $\mathrm{HF}_{\mathrm{model}}$ now contains the normalized [*i.e.*, $\mathrm{HF}_{\mathrm{model}}(T) = 1$] information of subperiod variability. For extremely dry climates (i.e., zero precipitation over the entire month), this could lead to an undetermined fraction. In practice, this can be avoided by specifying a very small minimum value (here 10^{-15}) for the normalization factor.
4) The target monthly total precipitation is obtained by multiplying the observed precipitation rate by the length of the current period:

$$P_{\mathrm{obs}} = T \times \mathrm{PR}_{\mathrm{obs}}, \qquad (2)$$

with P_{obs} the total precipitation over T and $\mathrm{PR}_{\mathrm{obs}}$ the precipitation rate.
5) The normalized cumulative sum coming from the reanalysis $\mathrm{HF}_{\mathrm{model}}$ is then multiplied by the monthly total precipitation from the observations $\mathrm{P}_{\mathrm{obs}}$ to produce a corrected cumulative sum:

$$\mathcal{P}_{\mathrm{CMT}}(t) = P_{\mathrm{obs}} \times \mathrm{HF}_{\mathrm{model}}(t). \qquad (3)$$

6) The precipitation rates are then obtained by applying differentiation in time to the corrected cumulative sum:

$$\mathrm{PR}_{\mathrm{CMT}} = \frac{\Delta \mathcal{P}_{\mathrm{CMT}}(t)}{\Delta t}. \qquad (4)$$

In this example, the obtained daily adjusted precipitation inherits the daily variability of the reanalysis precipitation rates while adding up to the monthly observed totals. By combining information from the two sources, the resulting precipitation dataset has now all the desired features.

3. Results

a. Precipitation dataset

Figure 2a shows the globally averaged precipitation rate in ERA-Interim with both daily and monthly values. As stated earlier, not only is ERA-Interim overestimating the total precipitation, but the time series present discontinuities or trends that are not observed in the monthly GPCP v2.3 data. Superposed onto GPCP in Fig. 2b is the Corrected Mean deTrended (hereafter CMT) precipitation dataset, resulting from the proposed method. The daily globally averaged precipitation is now exempt of any of the spurious trends of ERA-Interim and the monthly time series superposes exactly onto GPCP by design.

Figure 3 shows the zonally averaged precipitation rates over the 1998–2018 period in ERA-Interim, GPCP, and the CMT dataset. The CMT dataset reduces the bias in the equatorial band, which is responsible for the majority of the excess precipitation in ERA-Interim and slightly increased precipitation in the Northern Hemisphere subpolar gyre and the Southern Ocean, following GPCP. Although the properties of the CMT dataset is to reproduce the spatiotemporal averages of GPCP, its time variance (see Fig. 4) increase dramatically compared to GPCP. The latter has very low variability (under 15 $\mathrm{mm^2\ day^{-2}}$) with most of it concentrated in the intertropical convergence zone (ITCZ). The CMT dataset sees its variance rise to levels similar to ERA-Interim in all but the ITCZ, confirming it has captured the temporal variability from the reanalysis. In the ITCZ, the difference of variance between ERA-Interim (maximum of 85 $\mathrm{mm^2\ day^{-2}}$) and CMT (maximum of 50 $\mathrm{mm^2\ day^{-2}}$) can be explained by the bias reduction in this latitude band. Since ERA-Interim is overestimating the average precipitation rate in the ITCZ and precipitation rate is positive definite, reducing the peak monthly totals lead to the lower variance.

Since the observation-based datasets have uncertainties associated with the satellite retrievals and calibration to a sparse network of rain gauges, it is common practice to operate some data reductions in an attempt to reduce their impact, based on the assumption that the random part of errors will compensate. To assess the robustness of the method with coarser spatiotemporal resolution in the observational dataset, the algorithm is tested on two degraded versions of GPCP. CMT CR is built from a half-resolution GPCP (i.e., 5° × 5°) and CMT AN from an annual averages of GPCP, hence removing the seasonal cycle information from the observation dataset.

There is no notable difference when using the annual averages of GPCP to produce CMT AN on either the global average as shown by Fig. 2d, the zonal mean (Fig. 3), or the variance (Fig. 4). This suggests that the amplitude of the

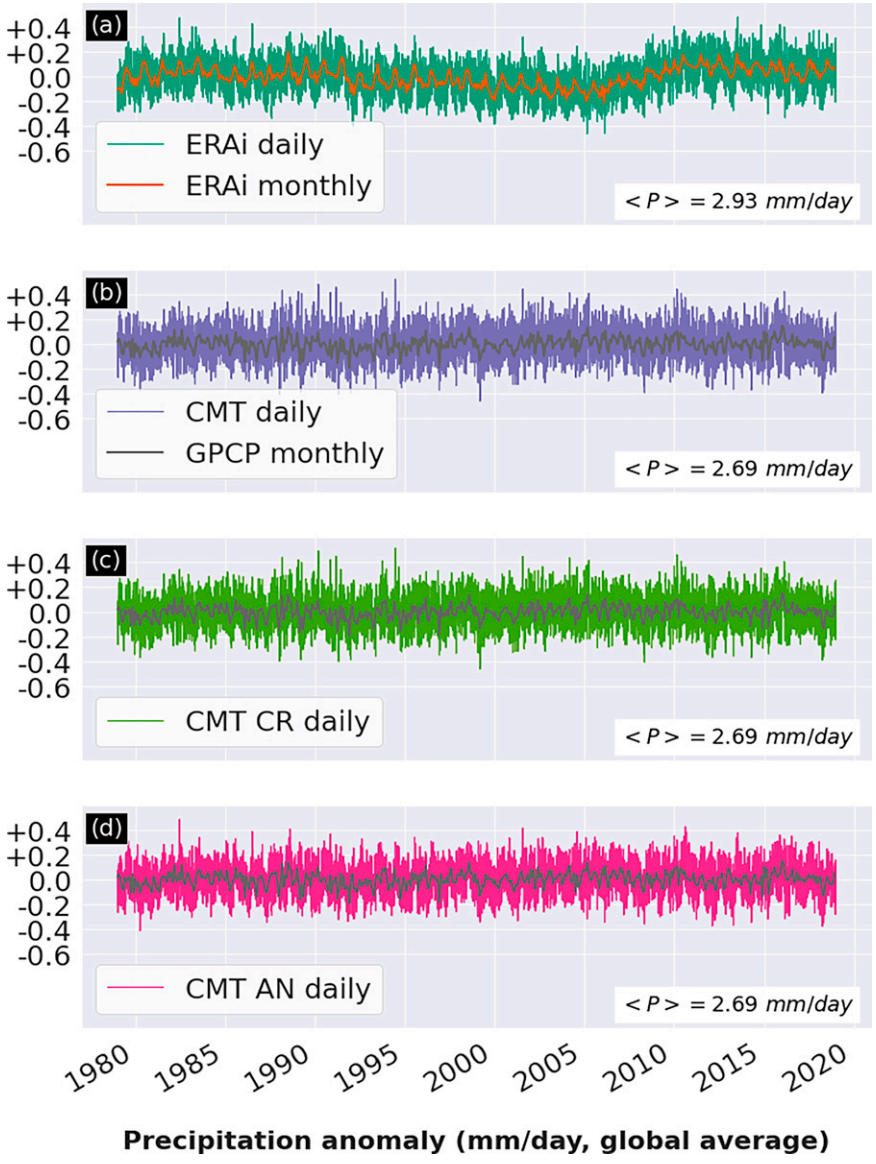

FIG. 2. Global mean precipitation (mm day^{-1}) in ERA-Interim, GPCP 2.3 and CMT products. (a) Daily and monthly ERA-Interim. Data are resampled to monthly for easier comparison with GPCP. (b) Daily CMT and monthly GPCP. Monthly CMT superposes exactly onto GPCP 2.3 by design. (c) Daily CMT from coarse resolution GPCP and (d) daily CMT from annual GPCP. In (c) and (d), monthly GPCP/CMT is superimposed.

seasonal cycle in ERA-Interim is in good agreement with the seasonal cycle of GPCP that has been filtered out and hence adjusting to the annual values produces similar results. Figure 5 confirms the hypothesis: the amplitude of the average seasonal cycle in ERA-Interim is well captured and is in good agreement with GPCP and the higher-resolution TRMM (here used for independent reference). When degrading the horizontal resolution of GPCP, there is no resulting difference in global average as shown in Fig. 2c and zonal average (Fig. 3) except for the enhanced staircase shape of CMT CR, resulting from the first-order remapping. The variance in CMT CR also stays consistent with CMT (Fig. 4). This shows the method proves robust against the lower spatial and temporal resolution of the observation dataset and hence can be used in a wider range of cases, including coarsely resolved observations.

The first-order conservative scheme introduces step discontinuities in the remapped GPCP which are visible on averages over periods greater than a month. However, the remapping, even from the $5^\circ \times 5^\circ$ grid, is not degrading the effective resolution of the obtained daily fields as can be seen in Fig. 6. In this zoom on a North Atlantic storm on 1 February 1979, the

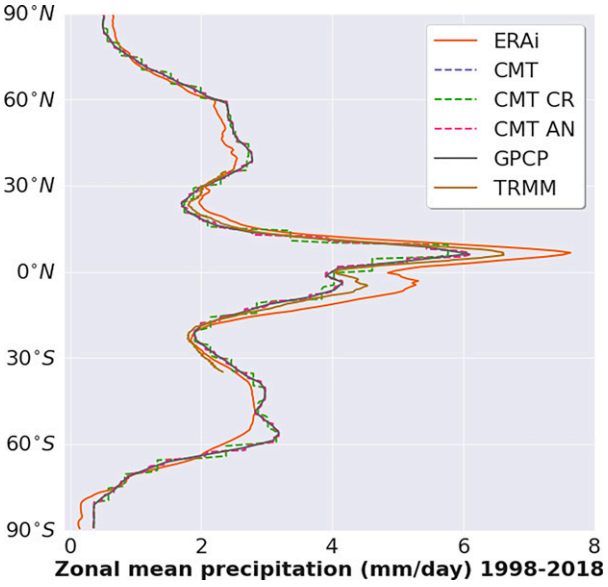

FIG. 3. Precipitation rates (mm day^{-1}, zonally averaged for 1998–2018) in CMT datasets, ERA-Interim, and observational estimates from GPCP and TRMM. The CMT family of datasets superpose onto GPCP, with small departures in the degraded spatiotemporal cases CMT CR and CMT AN.

core of the storm is intensified all while maintaining its spatial structure. The intensification makes it possible to meet the observed total precipitation at the end of the period, which allows the input of freshwater to the ocean at the desired fine spatial scales. In CMT AN, the intensification is lower because the observational constraint is not as tight. Because the method operates on monthly totals, both reanalysis and observations fields are reasonably smooth so their ratio is not very noisy and introduces little degradation from the remapping of the lower-resolution observation with a first-order conservative scheme.

b. *Numerical experiments*

The corrected precipitation dataset is compared to ERA-Interim and GPCP in a suite of forced ocean global numerical experiments (i.e., with a prescribed atmosphere, as opposed to a climate or Earth system model with a fully interactive atmosphere). The model used is the half-degree version of OM4 (Adcroft et al. 2019), in which the MOM6 ocean model is coupled with the SIS2 sea ice model. OM4 uses a vertical-remap vertical coordinate (Griffies et al. 2020), which allows vertical levels to move with the flow between remapping steps hence reducing diapycnal mixing compared to geopotential-based coordinates. The 75 vertical levels are following a hybrid coordinate, inspired by HYCOM (Chassignet et al. 2003; Bleck 2002), where geopotential surface levels transition to isopycnal layers at depth. The domain covers the entire globe with a resolution of 0.5°, refined at low latitudes to resolve equatorial dynamics and uses a tripolar grid to fully resolve the Arctic Ocean.

Although the numerics in the different ocean models differ significantly, the treatment of surface boundary conditions is usually very similar and involves some parameterization of the evaporation, heat, and momentum fluxes referred to as "bulk formulas." The most commonly used in forced ocean models are CORE (Large and Yeager 2004) and COARE (Fairall et al. 2003). Precipitation can be added either as a true freshwater flux (produces local sea level change) or as a virtual salt flux (only changes salinity), particularly in older formulations. In OM4, the atmospheric boundary condition is applied to the model by NOAA GFDL's FMS coupler, using the CORE bulk and precipitation is added as a freshwater flux along with river runoff. Imbalance in the freshwater budget (i.e., E–P–R) leads to large drift in global salinity and sea surface height. To prevent this from happening, MOM6 has a "zero net freshwater flux" algorithm that computes the excess/default freshwater at the current time step and redistributes it. This makes the strong assumption that all evaporated water is instantly compensated for, or equivalently that the atmospheric residence time is on the order of the coupling time step and land storage has no impact. However, the uncertainty associated with the intensity of evaporation in modeled air/sea bulk fluxes is quite large. Comparison to OAFlux (Yu et al. 2008) show that difference in evaporation between these experiments and the observational estimates is about 0.56 mm day^{-1} on average between 60°S and 60°N, and can be as great as 1 mm day^{-1} at low latitudes. Consequently, the readjustment of the freshwater flux can be justified as operating as a bias correction for the poorly constrained air/sea bulk fluxes.

The suite of experiments cover the 1979–2018 period and are using initial conditions derived from the *World Ocean Atlas 2013* (Locarnini et al. 2013; Zweng et al. 2013). The reference experiment (hereafter ERAi) uses the original ERA-Interim daily precipitation. The first sensitivity experiment (hereafter CMT) uses the proposed corrected precipitation daily CMT dataset. A second sensitivity experiment (GPCP) uses monthly GPCP v2.3 precipitation, linearly interpolated in time to daily values. The model requires to separate liquid (rain) and solid (snow) precipitation. Rainfall is thus computed as the difference between total precipitation and snowfall provided by ERA-Interim. In the case of GPCP, ERA-Interim snowfall needs to be averaged monthly before computing the rainfall. Failure to do so results in a mismatch in the temporal time scales of rain and snow hence producing overestimated rainfall totals and variance at latitudes where snow is present. The three aforementioned experiments are performed without balancing the net freshwater flux, the three complementary experiments using the freshwater balancing algorithm are labeled with the 0FW suffix. All other atmospheric variables are taken from ERA-Interim and interpolated to the model grid using either a first-order conservative method (for freshwater and radiative fluxes) or high-order "patch" method (for winds, air temperature and humidity) from the ESMF regridding library (Hill et al. 2004). Runoff is taken from the climatology of Dai and Trenberth (2002), a geothermal flux is added according to Davies (2013), and the sea surface salinity (SSS) is restored to the PHC2

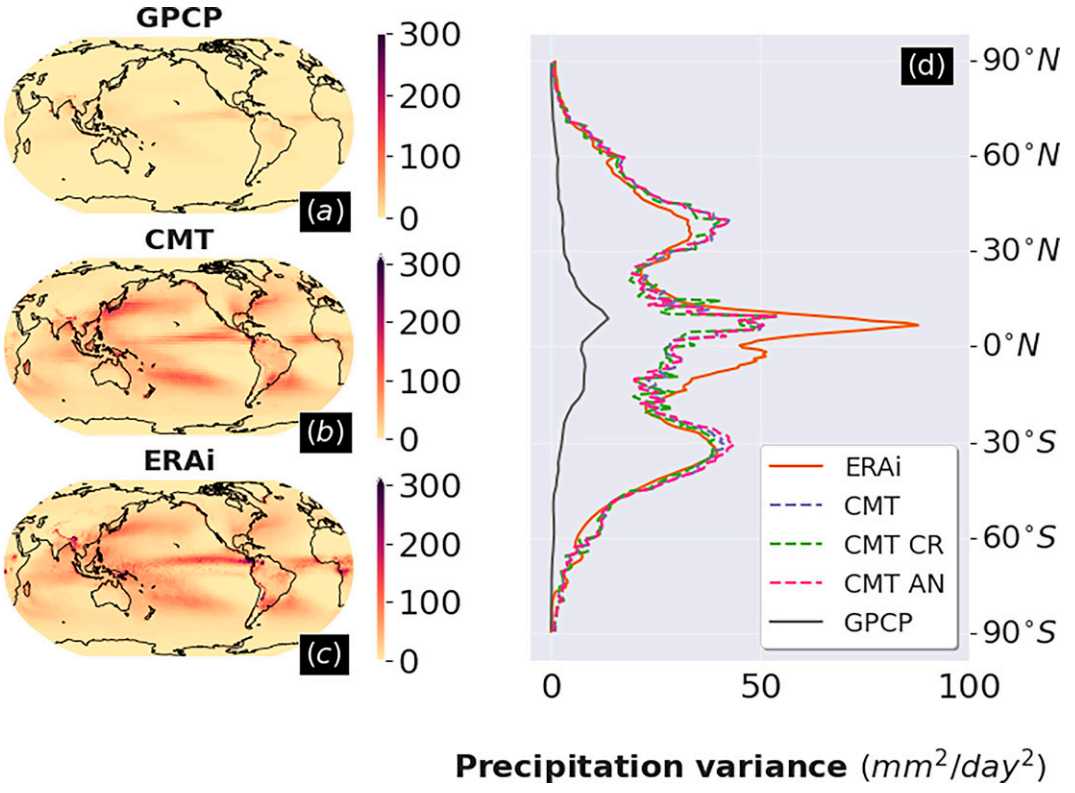

FIG. 4. Precipitation variance ($mm^2\ day^{-2}$) from daily time series in (a) GPCP, (b) CMT, and (c) ERA-Interim. (d) Zonal averages in the various datasets. Variance is consistent between the various versions of the CMT precipitations, largely increased compared to GPCP and on the same order of magnitude as ERA-Interim.

(Steele et al. 2001) climatology with a time scale of 0.1667 m day^{-1} [i.e., 50 m (300 days)$^{-1}$] time scale.

Figure 7 presents the globally averaged freshwater flux into the ocean for all experiments. As expected, experiments using the freshwater balancing algorithm show near-zero net freshwater flux into the ocean. Minimal deviations are possible due to the interaction with the sea ice model but show no interannual trend. All experiments start from ice-free conditions so the first years should be considered a "spinup" of the model and transients at the beginning of the time series are not relevant to the evolution of the E–P–R. The freshwater flux in the ERAi experiment clearly shows 3 phases: before 1992 it is near perfect balance before dropping to a 0.2 mm day^{-1} deficit until the mid-2000s and then trending up to reach quasi balance in the 2010s. This is consistent with the precipitation time series shown in Fig. 2a and indicate there is no compensating trend in evaporation, runoff having no interannual variability. The decline in precipitation over the 1992–2005 period results in a drop of almost 1 m in sea surface height (SSH) that partially recovers to −0.8 m by the end of the simulation. Over the 1992–2005 period, the ERAi experiment exhibits then a quasi-homogeneous spurious SSS trend of 0.08 PSU $decade^{-1}$ compared to the ERAi0FW experiment, despite the use of SSS restoring in both experiment. Such spurious trends are potentially badly damaging to the solution of the experiment and strengthen the need for balancing freshwater fluxes online when possible. CMT and GPCP show quasi-identical results (only differing by 0.5%). Using the observed mean precipitation results in a negative imbalance of −0.37 mm day^{-1} that remains quasi stationary. At the end of the experiment, the cumulative deficit in freshwater results in about −5 m loss of globally averaged SSH. Although this number is quite large and highlights the great uncertainties associated with closing the hydrological cycle of the ocean, the order of magnitude is consistent with what was obtained in other OM4 experiments with the JRA55-do forcing: +6 m of SSH after 60 years. Despite a larger deficit in freshwater, the SSS trend over the 1992–2005 period is on the same order of magnitude. This is due to the SSS restoring scheme acting as a limiter on how far away from the observations the SSS is allowed to depart. Lifting this constraint, for example to perform a regional freshwater balance analysis, would lead to largely overestimated SSS and associated trends.

Fortunately, because the deficit is quasi stationary, one could adjust the precipitation with a multiplicative factor, as is common practice with forced ocean models, in order to obtain the right freshwater balance. This is not done in the experiments as this type of tuning is typically specific to a given configuration, since it depends on the modeled evaporation, and of little interest in the context of this study. For example, in this configuration, adding the −0.37 mm day^{-1} deficit to the average 2.69 mm day^{-1} can be obtained with a multiplicative ratio of 1.14. This crude rescaling can amplify existing

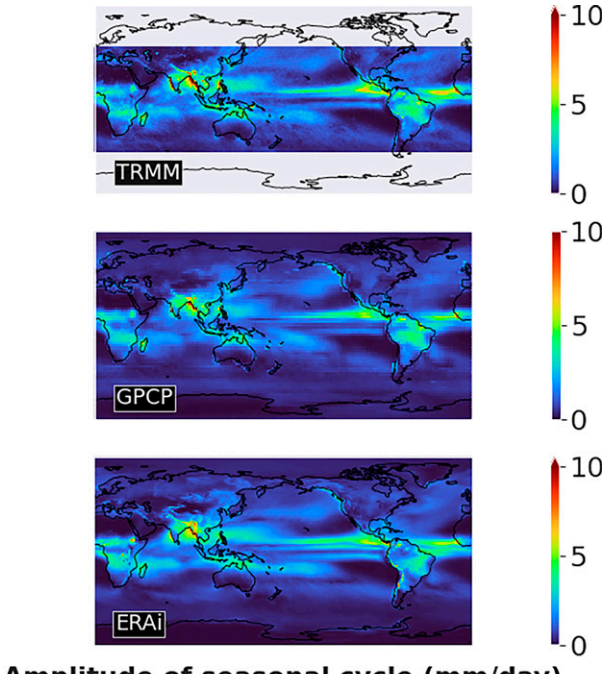

FIG. 5. Amplitude of the mean seasonal cycle (mm day^{-1}) in (top) TRMM, (middle) GPCP, and (bottom) ERA-Interim. The mean seasonal cycle is produced by averaging over the whole available period all values for each given month. The amplitude is then obtained with the standard deviation of the mean seasonal cycle.

trends in the dataset and does not account for regional distribution of uncertainties: Fig. 3 show that TRMM and GPCP estimates differ the most in the 10°S–10°N band by as much as 0.5 mm day^{-1}. Concentrating the adjustment on the low latitudes could provide better results, as previously proposed by Brodeau et al. (2010). An online freshwater balance algorithm can also solve this issue as shown in Fig. 8. Over the 1979–2018 period, CMT and GPCP have an average 0.39 PSU positive bias distributed over most of the oceans, where ERAi only has a 0.10 PSU mean bias, mainly driven by regional biases in the Arctic and in the North Atlantic. Forcing the freshwater fluxes to zero in CMT0FW and GPCP0FW prevent the large SSS drift and results in bias comparable to what is obtained in ERAi0FW, but with a slight degradation in the 30°S–30°N band. It is worth noting that the algorithm is not intended to be an SSS bias correction since large difference resulting from poorly resolved processes, such as the Gulf Stream path, will still exist.

Since experiments forced by GPCP and CMT precipitation lead to similar freshwater fluxes and SSS bias, one could be tempted to simply use GPCP. In addition, SSS variance is dominated by the seasonal cycle so results for all datasets do not show major differences. Figure 9 shows the average SSS standard deviation at the submonthly time scale: the standard deviation is computed for each month and then averaged over all months of the simulations and this makes it possible to remove the seasonal component of the SSS variability. Figures 9a and 9b show that the day to day variability in precipitation in ERA-Interim and CMT is associated with an increased variability of the SSS, except in parts of the western equatorial Pacific and northern Indian Oceans, and particularly at low and midlatitudes compared to the experiment forced with GPCP. Because ERA-Interim has different precipitation rates than GPCP, the resulting submonthly standard deviation in Fig. 9a is the superposition of the effect of daily versus monthly forcing and of the precipitation bias. Since ERA-Interim has overestimated precipitation in the equatorial band, the SSS variability is driven up by the larger rainfall rates. On the contrary, CMT and GPCP sum up to the same monthly total precipitation, which lessen the extent of the areas showing increased SSS variability at the submonthly time scale. These are concentrated over the subtropical gyres and near the eastern equatorial Pacific and Atlantic and can be as large as 0.02 PSU in standard deviation. Figures 9c and 9d show that the freshwater balancing algorithm does not have much impact on the SSS variability in the ERA-Interim-forced experiments but have a quite large impact in the CMT-forced and GPCP-forced ones. Since the net freshwater flux with ERA-Interim precipitation is closer to balance, the algorithm redistribute a smaller quantity of freshwater than in the CMT0FW and GPCP0FW experiments. The redistribution of freshwater in the latter experiments tends to produce changes in SSS variability, particularly in the Southern Ocean and the North Atlantic. This suggests that the use of the online freshwater balancing in conjunction with precipitation datasets that are far from balance with evaporation, such as CMT or JRA55-do, can spur changes in SSS variability that are on the same order of magnitude than daily variability.

4. Discussion

As the numerical experiments demonstrate, adjusting the precipitation is not sufficient to obtain good agreement between modeled and observed SSS. Aside from errors arising from the limitations in the treatment of dynamics and thermodynamics in numerical models of the ocean, uncertainties in the freshwater fluxes also complicate the task at hand. The first source of uncertainty originates from the treatment of river discharge/runoff. For lack of an interannual dataset covering the whole period, the experiments are forced with the Dai and Trenberth (2002) monthly climatology. Their estimates are averaged over the 1950–99 period and represent a positive freshwater flux into the ocean of about 37 288 km^3 yr^{-1} [i.e., 0.28 mm day^{-1} or 1.18 Sv (1 Sv $\equiv 10^6$ m^3 s^{-1})]. The lack of interannual variability in the river discharge could prevent to perfectly close the hydrological cycle if the other fluxes were well modeled (evaporation) or prescribed (precipitation). Since the order of magnitude of river input is equivalent to roughly 10% of the precipitation and evaporation rates, the errors on the former are overshadowed by uncertainties of the latter. Evaporation rates in the experiments are stronger than the observational estimates of OAFlux (Yu et al. 2008): between 60°S and 60°N, the model has on average an evaporation of 3.88 mm day^{-1}, which is 0.56 mm day^{-1} greater than observations. Since the evaporation has to be parameterized

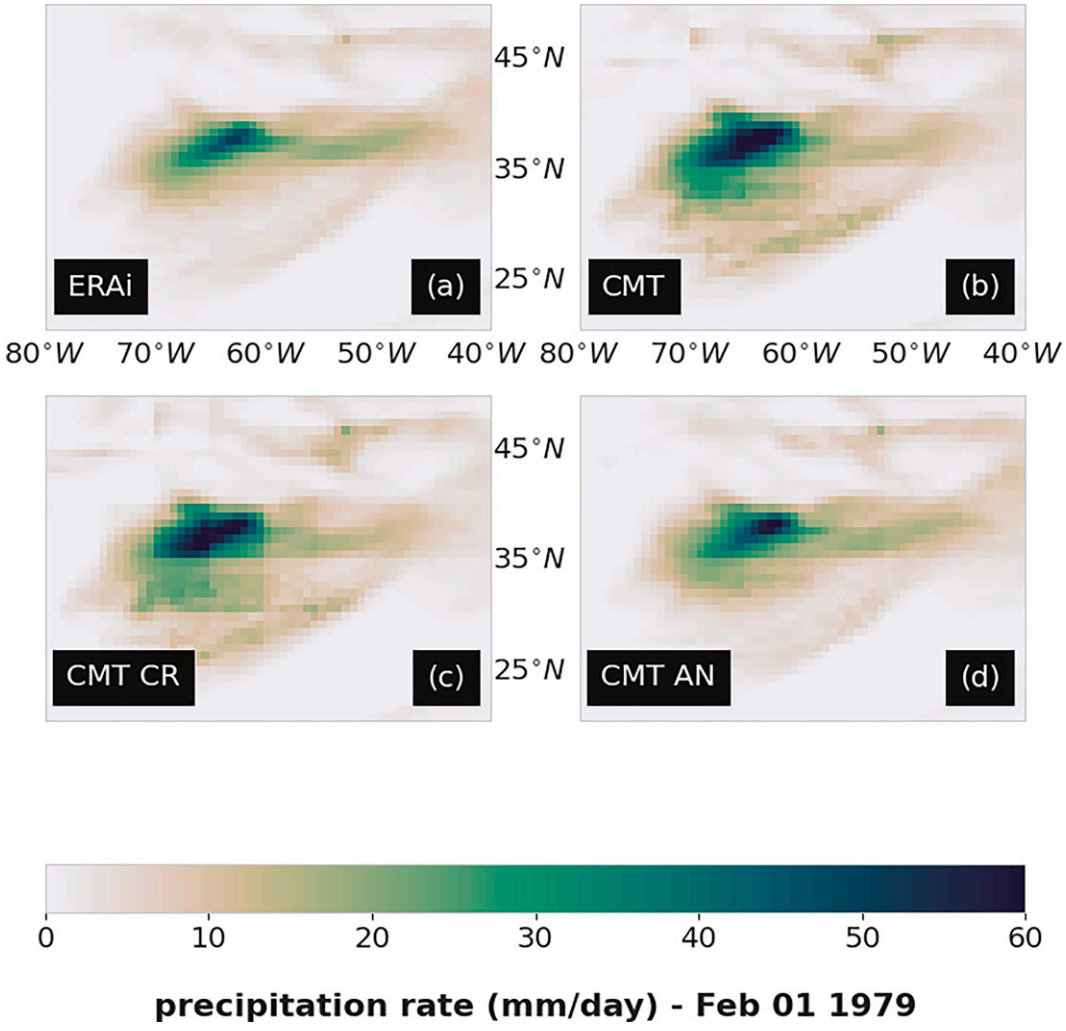

FIG. 6. Precipitation rate (mm day^{-1}) on 1 Feb 1979, zoom on a North Atlantic storm. The original ERA-Interim is compared to the solutions of the method, with or without spatiotemporal degradation of observational constraints.

using the air/sea CORE (Large and Yeager 2004) bulk formula, errors in modeled SST and surface variables (winds, humidity) from the ERA-Interim reanalysis can lead to errors in the evaporative flux. Performance of the chosen bulk formula can also be responsible for biases. Even though this formulation is among the most used in the ocean modeling community, the parameterization of air/sea fluxes is an active field of research and other formulations have been proposed,

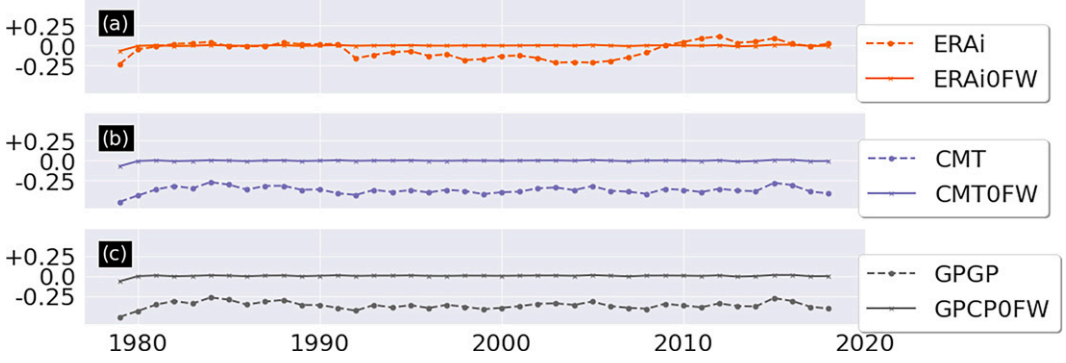

FIG. 7. Globally averaged net freshwater fluxes in OM4 experiments (mm day^{-1}) forced by (a) ERA-Interim, (b) CMT, and (c) GPCP. Experiments with 0FW suffix use the "zero net freshwater flux" algorithm.

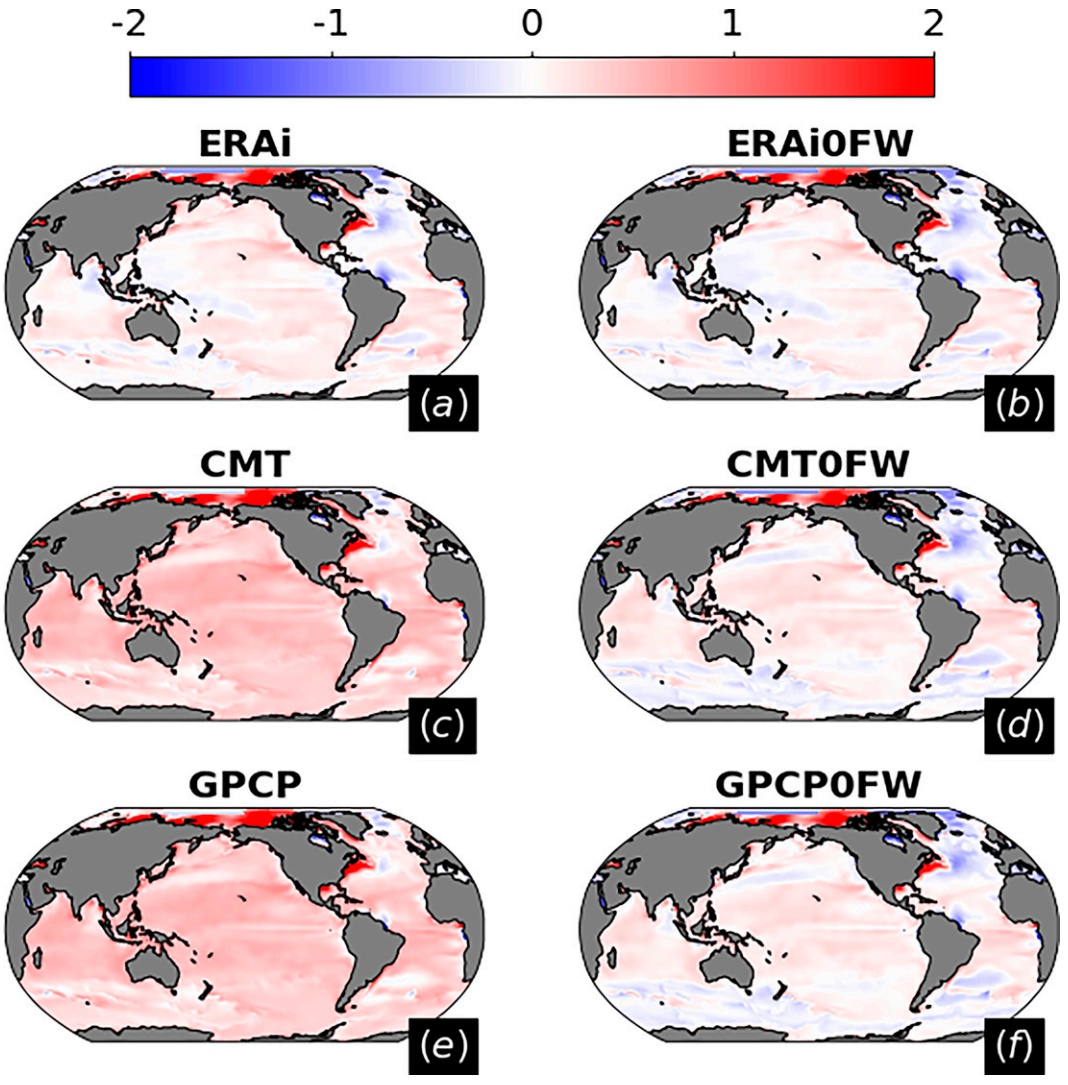

FIG. 8. Sea surface salinity annual bias with respect to *World Ocean Atlas 2013* in OM4 experiments forced by (a),(b) ERA-Interim, (c),(d) CMT, and (e),(f) GPCP. Experiments (a) ERAi, (c) CMT, (e) GPCP do not use the "zero net freshwater" algorithm and hence have larger SSS biases than experiments (b) ERAi0FW, (d) CMT0FW, and (f) GPCP0FW.

most notably by Fairall et al. (2003) and Edson et al. (2013). Rectifying the precipitation is also complicated by the remaining uncertainties on what its true value should be. Discrepancies in the tropics between the GPCP and TRMM estimates can be clearly seen in Fig. 3. Based on the intercomparison of the two datasets, Adler et al. (2012) provides an estimate of ±7% error on GPCP in the tropics [revised from ±3% in Adler et al. (2009)] and 7%–9% globally, which represents about 0.18–0.24 mm day^{-1}. This remains smaller than the differences between GPCP and the modeled precipitation.

The well-informed numerical oceanographer would be able to blend observational datasets based on their qualities, tune totals to balance freshwater fluxes, and use the method described here to produce an updated precipitation dataset free of spurious trends for which the mean values are appropriate for the application considered. Although it has been shown not to degrade significantly the solution, the first-order remapping could be replaced by the second-order remapping now available from Hill et al. (2004). The online "zero net freshwater algorithm" certainly proves useful in preventing large drifts in SSH but may not be applicable in all cases (e.g., regional model) and is shown to create spurious SSS variability that can result in unintended consequences, particularly in areas sensitive to small changes in surface properties. Since the phenomenon increases with the amplitude of the freshwater imbalance, adjusting precipitation datasets so that the freshwater budget is close to balance may improve performance of the model. ERA-Interim performs relatively well in that respect since its excess precipitation compensates for the

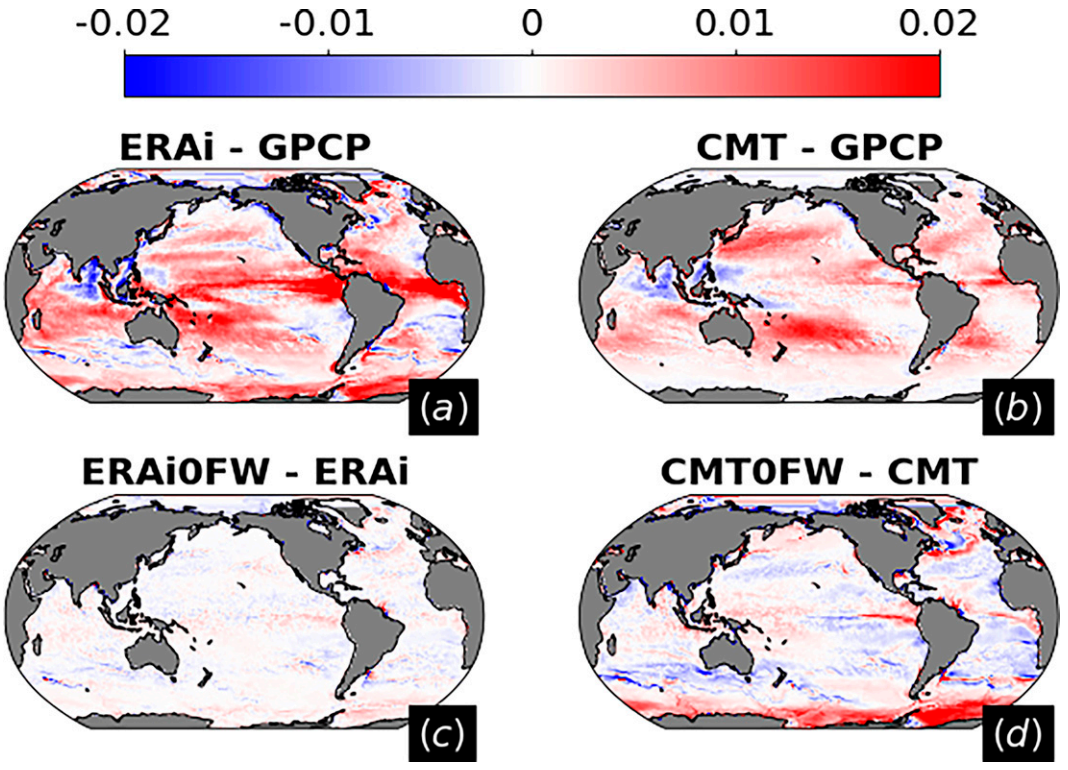

FIG. 9. Difference in sea surface salinity standard deviation (mm day^{-1}) at submonthly time scales between OM4 experiments. (a),(b) Difference between ERA-Interim-forced and CMT-forced compared to GPCP-forced. (c),(d) Impact of the "zero net freshwater" algorithm using the same precipitation dataset for ERA-Interim and CMT.

excess evaporation in the bulk and the freshwater budget is close to balance, even without the online correction. Other datasets, further away from balance, may not perform as well, as seen for the proposed CMT dataset.

5. Conclusions

A simple method can be used to efficiently remedy the biases and spurious trends in a precipitation dataset using constraints from an observational dataset of lower resolution in time and space. This makes it possible to force an ocean model with high-frequency precipitation while being consistent with observed totals. The method does not suffer from the degradation in space and time of the observational dataset and provides robust results. However, an observation-based dataset is required over the considered period for the method to be applicable. When applied to a global ocean model, it highlights the difficulty to balance freshwater due to the large uncertainties in these fluxes. Nonetheless the mean solution obtained with the CMT dataset show consistency with results obtained with GPCP, while providing extra information at the intramonthly time scales. Although this method is not designed to close the freshwater budget, it can provide a solid starting point for subsequent tuning.

Although forced ocean models provide an imperfect framework to answer scientific questions, their usefulness have been demonstrated over and over in past decades. Fully coupled Earth system models are either not well suited or too expensive for some applications such as high-resolution ocean or regional studies. The ability to control the surface boundary condition to study ocean response to atmospheric perturbations is also a very desirable feature for oceanographers. For all these reasons, it is important to continue to improve the treatment of the surface boundary condition in forced ocean models. This effort can be directed at improving available atmospheric datasets (Tsujino et al. 2018; Brodeau et al. 2010; Large and Yeager 2004; Dussin and Barnier 2013), advancing our understanding of air–sea fluxes (Fairall et al. 2003; Edson et al. 2013; Bao et al. 2011), how to represent them in ocean models (Barnier 1998; Brodeau et al. 2017) and using climate models to provide additional constraints (Harrison et al. 2022).

Acknowledgments. This research from the Geophysical Fluid Dynamics Laboratory is supported by NOAA's Science Collaboration Program and administered by UCAR's Cooperative Programs for the Advancement of Earth System Science (CPAESS) under Awards NA16NWS4620043 and NA18NWS4620043B. Many thanks to John Krasting, Matthew Harrison, Enrique Curchitser, and Stephen Griffies for their insightful comments which helped significantly improve the manuscript. I would also like to thank the three anonymous reviewers for thoroughly reading this manuscript, which

made it possible to catch a few lingering mistakes and clarify certain points of the methodology.

Data availability statement. The CMT dataset is available on Zenodo (DOI 10.5281/zenodo.2614004) and the source code is available on GitHub at https://github.com/raphaeldussin/dev_forcings/tree/master/precip_erainterim_correction_gpcp and https://github.com/raphaeldussin/runs_MOM6_dev_forcing.

REFERENCES

Adcroft, A., and Coauthors, 2019: The GFDL global ocean and sea ice model OM4.0: Model description and simulation features. *J. Adv. Model. Earth Syst.*, **11**, 3167–3211, https://doi.org/10.1029/2019MS001726.

Adler, R. F., and Coauthors, 2003: The version-2 Global Precipitation Climatology Project (GPCP) monthly precipitation analysis (1979–present). *J. Hydrometeor.*, **4**, 1147–1167, https://doi.org/10.1175/1525-7541(2003)004<1147:TVGPCP>2.0.CO;2.

——, J.-J. Wanf, G. Gu, and G. J. Huffman, 2009: A ten-year tropical rainfall climatology based on a composite of TRMM products. *J. Meteor. Soc. Japan*, **87A**, 281–293, https://doi.org/10.2151/jmsj.87A.281.

——, G. Gu, and G. J. Huffman, 2012: Estimating climatological bias errors for the Global Precipitation Climatology Project (GPCP). *J. Appl. Meteor. Climatol.*, **51**, 84–99, https://doi.org/10.1175/JAMC-D-11-052.1.

Bao, J.-W., C. W. Fairall, S. Michelson, and L. Bianco, 2011: Parameterizations of sea-spray impact on the air–sea momentum and heat fluxes. *Mon. Wea. Rev.*, **139**, 3781–3797, https://doi.org/10.1175/MWR-D-11-00007.1.

Barnier, B., 1998: Forcing the ocean. *Ocean Modeling and Parameterization*, Springer, 45–80.

Bleck, R., 2002: An oceanic general circulation model framed in hybrid isopycnic-Cartesian coordinates. *Ocean Modell.*, **4**, 55–88, https://doi.org/10.1016/S1463-5003(01)00012-9.

Brodeau, L., B. Barnier, A.-M. Treguier, T. Penduff, and S. Gulev, 2010: An ERA40-based atmospheric forcing for global ocean circulation models. *Ocean Modell.*, **31**, 88–104, https://doi.org/10.1016/j.ocemod.2009.10.005.

——, ——, S. K. Gulev, and C. Woods, 2017: Climatologically significant effects of some approximations in the bulk parameterizations of turbulent air–sea fluxes. *J. Phys. Oceanogr.*, **47**, 5–28, https://doi.org/10.1175/JPO-D-16-0169.1.

Chassignet, E. P., L. T. Smith, G. R. Halliwell, and R. Bleck, 2003: North Atlantic simulations with the Hybrid Coordinate Ocean Model (HYCOM): Impact of the vertical coordinate choice, reference pressure, and thermobaricity. *J. Phys. Oceanogr.*, **33**, 2504–2526, https://doi.org/10.1175/1520-0485(2003)033<2504:NASWTH>2.0.CO;2.

Dai, A., 2006: Precipitation characteristics in eighteen coupled climate models. *J. Climate*, **19**, 4605–4630, https://doi.org/10.1175/JCLI3884.1.

——, and K. E. Trenberth, 2002: Estimates of freshwater discharge from continents: Latitudinal and seasonal variations. *J. Hydrometeor.*, **3**, 660–687, https://doi.org/10.1175/1525-7541(2002)003<0660:EOFDFC>2.0.CO;2.

Davies, J. H., 2013: Global map of solid Earth surface heat flow. *Geochem. Geophys. Geosyst.*, **14**, 4608–4622, https://doi.org/10.1002/ggge.20271.

Dee, D. P., and Coauthors, 2011: The ERA-Interim reanalysis: Configuration and performance of the data assimilation system. *Quart. J. Roy. Meteor. Soc.*, **137**, 553–597, https://doi.org/10.1002/qj.828.

Delcroix, T., C. Henin, V. Porte, and P. Arkin, 1996: Precipitation and sea-surface salinity in the tropical Pacific Ocean. *Deep-Sea Res. I*, **43**, 1123–1141, https://doi.org/10.1016/0967-0637(96)00048-9.

Dussin, R., and B. Barnier, 2013: The making of DRAKKAR Forcing Set 5.1. MEOM/LEGI Tech. Rep., 40 pp., https://www.drakkar-ocean.eu/publications/reports/dfs5-1-report.

Edson, J. B., and Coauthors, 2013: On the exchange of momentum over the open ocean. *J. Phys. Oceanogr.*, **43**, 1589–1610, https://doi.org/10.1175/JPO-D-12-0173.1.

Fairall, C. W., E. F. Bradley, J. Hare, A. A. Grachev, and J. B. Edson, 2003: Bulk parameterization of air–sea fluxes: Updates and verification for the COARE algorithm. *J. Climate*, **16**, 571–591, https://doi.org/10.1175/1520-0442(2003)016<0571:BPOASF>2.0.CO;2.

Griffies, S. M., and Coauthors, 2009: Coordinated Ocean-Ice Reference Experiments (COREs). *Ocean Modell.*, **26**, 1–46, https://doi.org/10.1016/j.ocemod.2008.08.007.

——, A. Adcroft, and R. W. Hallberg, 2020: A primer on the vertical Lagrangian-remap method in ocean models based on finite volume generalized vertical coordinates. *J. Adv. Model. Earth Syst.*, **12**, e2019MS001954, https://doi.org/10.1029/2019MS001954.

Harrison, M. J., A. J. Adcroft, R. Hallberg, and O. Sergienko, 2022: Improved surface mass balance closure in ocean hindcast simulations. *J. Adv. Model. Earth Syst.*, **14**, e2021MS002888, https://doi.org/10.1029/2021MS002888.

Hill, C., C. DeLuca, M. Suarez, and A. R. da Silva, 2004: The architecture of the Earth system modeling framework. *Comput. Sci. Eng.*, **6**, 18–28, https://doi.org/10.1109/MCISE.2004.1255817.

Huffman, G. J., and Coauthors, 2007: The TRMM Multisatellite Precipitation Analysis (TMPA): Quasi-global, multiyear, combined-sensor precipitation estimates at fine scales. *J. Hydrometeor.*, **8**, 38–55, https://doi.org/10.1175/JHM560.1.

Kanamitsu, M., W. Ebisuzaki, J. Woollen, S.-K. Yang, J. Hnilo, M. Fiorino, and G. Potter, 2002: NCEP–DOE AMIP-II reanalysis (R-2). *Bull. Amer. Meteor. Soc.*, **83**, 1631–1644, https://doi.org/10.1175/BAMS-83-11-1631.

Killworth, P. D., 1996: Time interpolation of forcing fields in ocean models. *J. Phys. Oceanogr.*, **26**, 136–143, https://doi.org/10.1175/1520-0485(1996)026<0136:TIOFFI>2.0.CO;2.

Large, W. G., and S. G. Yeager, 2004: Diurnal to decadal global forcing for ocean and sea-ice models: The data sets and flux climatologies. NCAR Tech. Note NCAR/TN-460+STR, 105 pp., https://doi.org/10.5065/D6KK98Q6.

——, and ——, 2009: The global climatology of an interannually varying air–sea flux data set. *Climate Dyn.*, **33**, 341–364, https://doi.org/10.1007/s00382-008-0441-3.

Locarnini, R., and Coauthors, 2013: *Temperature*. Vol. 1, *World Ocean Atlas 2013*, NOAA Atlas NESDIS 73, 40 pp., http://data.nodc.noaa.gov/woa/WOA13/DOC/woa13_vol1.pdf.

Steele, M., R. Morley, and W. Ermold, 2001: PHC: A global ocean hydrography with a high-quality Arctic ocean. *J. Climate*, **14**, 2079–2087, https://doi.org/10.1175/1520-0442(2001)014<2079:PAGOHW>2.0.CO;2.

Stephens, G. L., and Coauthors, 2010: Dreary state of precipitation in global models. *J. Geophys. Res.*, **115**, D24211, https://doi.org/10.1029/2010JD014532.

Tapiador, F. J., R. Roca, A. Del Genio, B. Dewitte, W. Petersen, and F. Zhang, 2019: Is precipitation a good metric for model performance? *Bull. Amer. Meteor. Soc.*, **100**, 223–233, https://doi.org/10.1175/BAMS-D-17-0218.1.

Tsujino, H., and Coauthors, 2018: JRA-55 based surface dataset for driving ocean–sea-ice models (JRA55-do). *Ocean Modell.*, **130**, 79–139, https://doi.org/10.1016/j.ocemod.2018.07.002.

——, and Coauthors, 2020: Evaluation of global ocean–sea-ice model simulations based on the experimental protocols of the Ocean Model Intercomparison Project phase 2 (OMIP-2). *Geosci. Model Dev.*, **13**, 3643–3708, https://doi.org/10.5194/gmd-13-3643-2020.

Uppala, S., 2001: ECMWF Reanalysis 1957-2001, ERA-40. ECMWF ERA-40 Project Rep. 3, 10 pp., https://www.ecmwf.int/node/12879.

Xie, P., and P. A. Arkin, 1997: Global precipitation: A 17-year monthly analysis based on gauge observations, satellite estimates, and numerical model outputs. *Bull. Amer. Meteor. Soc.*, **78**, 2539–2558, https://doi.org/10.1175/1520-0477(1997)078<2539:GPAYMA>2.0.CO;2.

Yu, L., X. Jin, and R. Weller, 2008: Multidecade global flux datasets from the objectively analyzed air-sea fluxes (OAFlux) project: Latent and sensible heat fluxes, ocean evaporation, and related surface meteorological variables. Woods Hole Oceanographic Institution OAFlux Project Tech. Rep. OA-2008-01, 64 pp.

Zweng, M., and Coauthors, 2013: *Salinity*. Vol. 2, *World Ocean Atlas 2013*, NOAA Atlas NESDIS 74, 39 pp., http://data.nodc.noaa.gov/woa/WOA13/DOC/woa13_vol2.pdf.